PCCP

Accepted Manuscript

This is an *Accepted Manuscript*, which has been through the Royal Society of Chemistry peer review process and has been accepted for publication.

Accepted Manuscripts are published online shortly after acceptance, before technical editing, formatting and proof reading. Using this free service, authors can make their results available to the community, in citable form, before we publish the edited article. We will replace this *Accepted Manuscript* with the edited and formatted *Advance Article* as soon as it is available.

You can find more information about *Accepted Manuscripts* in the [Information for Authors](#).

Please note that technical editing may introduce minor changes to the text and/or graphics, which may alter content. The journal's standard [Terms & Conditions](#) and the [Ethical guidelines](#) still apply. In no event shall the Royal Society of Chemistry be held responsible for any errors or omissions in this *Accepted Manuscript* or any consequences arising from the use of any information it contains.

1 # First evidence of the dramatic enhancement of the

2 # reactivity of methyl formate (HC(O)OCH$_3$) with

3 # OH at temperatures of the interstellar medium: A

4 # gas-phase kinetic study between 22 K and 64 K

5 *E. Jiménez[1,2,]*, M. Antiñolo[1,2], B. Ballesteros,[1,2] A. Canosa,[3] and J. Albaladejo[1,2]*

6 [1] Departamento de Química Física. Facultad de Ciencias y Tecnologías Químicas.

7 Universidad de Castilla-La Mancha, Avda. Camilo José Cela, s/n. 13071 Ciudad Real,

8 Spain

9 [2] Instituto de Combustión y Contaminación Atmosférica (ICCA). Universidad de Castilla-

10 La Mancha, Avda. Moledores s/n. 13071 Ciudad Real, Spain

11 [3] Département de Physique Moléculaire, Institut de Physique de Rennes, UMR CNRS-UR1

12 6251, Université de Rennes 1, Campus de Beaulieu, 263 Avenue du Général Leclerc,

13 35042 Rennes Cedex, France

14

15 **Corresponding Author**

16 * Phone: +34 926 29 53 00, Fax: +34 926 29 53 18, e-mail: Elena.Jimenez@uclm.es

17   **ABSTRACT.** Gas-phase chemistry of neutral-neutral reactions of interest in the interstellar

18   medium (ISM) is poorly-understood. The rate coefficients (k_{OH}) for the majority of the

19   reactions of hydroxyl (OH) radicals with interstellar oxygenated species are unknown at

20   temperatures of the ISM. In this work, we present the first determination of k_{OH} for

21    $HC(O)OCH_3$ between (22.4±1.4) and (64.2±1.7)K. The CRESU (French acronym for

22   *Cinétique de Réaction en Ecoulement Supersonique Uniforme* or Reaction Kinetics in a

23   Uniform Supersonic Flow) technique was used to create a chemical reactor with a uniform

24   temperature and gas density and the pulsed laser photolysis/laser induced fluorescence

25   technique was used to generate OH radicals and to monitor their temporal profile. It was

26   observed that $k_{OH}(T)$ increases one order of magnitude in only ~40K

27   ($k_{OH}(T=22K)=(1.19±0.36)×10^{-10}$ cm^{3}s^{-1} and $k_{OH}(T=64K)=(1.16±0.12)×10^{-11}$ cm^{3}s^{-1}), and ~3

28   orders of magnitude with respect to $k_{OH}(T=298K)$. This reaction is a very efficient loss

29   route for $HC(O)OCH_3$ in the gas phase and may have a great impact on the interpretation

30   by astrophysical models of the $HC(O)OCH_3$ abundances in cold regions of the ISM.

31

1 Introduction

Observations of interstellar material started in the last century and nowadays more than 180 species, besides the most abundant H_2 and He, are confirmed to be present in the interstellar medium (ISM). Among them, radicals and neutral molecular species containing C, H, and O, such as alcohols, aldehydes, acids and esters, have been detected in dense molecular clouds (T = 10-100 K) and star-forming regions (T > 100 K). For instance, hydroxyl (OH) radicals and methyl formate ($HC(O)OCH_3$) were detected in the ISM molecular clouds.[1-8] The observed abundances relative to H_2 in hot cores and hot corinos were reported to be 3×10^{-8} and 1.4×10^{-8} (in Orion), 4×10^{-7} (in IRAS 16293-2422) and 7×10^{-7} (IRAS 4A). The diverse abundances can be attributed to differences in physical conditions (for instance, the temperature evolution during the warm-up timescale of the object) that affect the chemistry. Recent detections of methyl formate in colder objects, such as protostars Barnard 1b,[9] in cold environment of IRAS 16293-2422[10] and prestellar cores[11] demonstrate that understanding the formation of complex organic molecules (COMs) in these environments is one of the key issues to model properly the observed abundances of these molecules in the ISM.

The formation mechanism of $HC(O)OCH_3$ has been the subject of several studies,[12-19] but it is not yet well-understood. In hot cores and corinos, it is believed that some organic molecules are formed in grain-surfaces and subsequently injected into the gas phase during the warm-up phase. Once in the gas-phase these molecules are ionized being the precursors of other COMs, such as $HC(O)OCH_3$. Some models exclusively use gas phase reactions, for example, Horn et al.[12] proposed several formation routes for $HC(O)OCH_3$ via the recombination reaction of a protonated and a neutral species followed

55   by dissociative recombination with electrons. Nevertheless, this gas-phase chemical model

56   underpredicts the observed abundances of $HC(O)OCH_3$ in hot cores at $T\sim100$ K. More

57   recently, Balucani *et al.*[18] proposed a new chemical model for the gas-phase formation of

58   $HC(O)OCH_3$ in colder environments, based on the fact that ejection of CH_3OH takes place

59   from the outer shell of the cold prestellar core ($T\sim10$ K) contrary to previous assumptions.

60   These authors concluded that although the gas-phase formation of methyl formate cannot

61   be neglected, grain-surface formation is an important formation route for this COM. In gas-

62   grain models, it is assumed that the formation of $HC(O)OCH_3$ occurs via the reaction of

63   methoxy (CH_3O) and formyl (HCO) at temperatures around 30-40 K, afterwards it is

64   gradually evaporated into the gas phase.[13,14] The evidence that the CH_3O+HCO reaction

65   can occur in interstellar granular ices was experimentally proven by Bennett and Kaiser[15]

66   and Modica and Palumbo.[19] What is clear is that gas-phase formation of $HC(O)OCH_3$ is

67   interconnected with grain-surface formation, but what about the removal processes of

68   $HC(O)OCH_3$ in the gas phase at temperatures of cold objects? Evidently, the gas-phase loss

69   processes of this COM need to be included as well in chemical models to properly interpret

70   the observed abundances. Among them, ultraviolet (UV) photodissociation processes and

71   radical-COM reactions have to be taken into account in the models. UV photodissociation

72   of methyl formate has been investigated at room temperature (yielding mainly CH_3O and

73   HCO radicals),[20-22] while the chemical kinetics for the gas-phase reaction of OH radicals

74   with methyl formate,

75        $$OH + HC(O)OCH_3 \rightarrow \text{Products} \qquad k_{OH}, \qquad (1)$$

76   has been investigated at temperatures between 233 and 1500 K and pressures between 0.4

77   and 1.63 atm.[23-29] Up to date no chemical kinetic studies of $HC(O)OCH_3$ have been

78   reported at lower temperatures. Therefore, the aim of this work is to report for the first time

79   k_{OH} for reaction (1) between 22 and 64 K, temperatures of interest in the ISM.

80   **2 Experimental**

81   **2.1 General Aspects**

82   The CRESU system employed in this work is schematically shown in **Figure 1**. This setup,

83   which was exhaustively described by Jiménez *et al.*[30], couples the uniform supersonic gas

84   expansion technique, to achieve the ultra-low temperatures needed for determining $k_{OH}(T)$

85   between 22 and 64 K, and the pulsed laser photolysis-laser induced fluorescence (PLP-LIF)

86   kinetic technique.

87   Ultra-low temperatures are achieved by the isentropic expansion of a gas mixture,

88   consisting in the buffer gas, the OH-precursor (H_2O_2), and diluted $HC(O)OCH_3$, through a

89   Laval nozzle from a high pressure reservoir (P_{res}) to a vacuum chamber (P_{cham}). In this

90   work, the Laval nozzle described in reference 30 was used for getting all temperatures. This

91   nozzle was initially designed to obtain 22 K in helium (conditions **A** in **Table 1**). However,

92   calculations performed with a home-made program, which take into account the existing

93   profile of the divergent-convergent nozzle, indicate that other uniform supersonic flows

94   could be obtained by varying the pressure and temperature conditions as well as the mass

95   flow rates (F) for different buffer gases (helium, nitrogen or a mixture of both). The

96   optimal P_{res} and P_{cham} and ranges of the calibrated mass flows for the buffer gas (F_{buffer}), the

97   buffer gas through the H_2O_2 bubbler ($F_{H_2O_2}$) and diluted $HC(O)OCH_3$ (F_R) are summarized

98   in **Table 1**. In the case of conditions **B** (see **Table 1**), the buffer gas is a mixture of He

99   (40%) and N_2 (60%) independently introduced in the reservoir. As described elsewhere,[30-32]

100 the buffer gas is flowing through a glass bubbler containing a pre-concentrated aqueous

101 solution of H_2O_2. In case **B**, N_2 was only flowed through the bubbler. Diluted methyl

102 formate was prepared in two 20-L storage bulbs connected in series. Mixing ratios of

103 methyl formate (*f*) in the 40-L storage bulb ranged from *ca.* 2×10^{-3} to 8×10^{-2}.

104   The aerodynamic chopper[30] (rotary disk at 10 Hz) placed at the divergent part of the

105 Laval nozzle was operational under experimental conditions **A** (hitherto pulsed mode for

106 getting 22 K). The pulsing of the gas was not necessary to achieve higher temperatures

107 (conditions **B-D**, continuous mode), since the required mass flows and working pressures

108 were accessible with the pumping capacities of our experimental system. In the generated

109 supersonic gas flow the temperature (*T*), the total gas density (*n*), and the velocity are

110 uniform along the flow.

111

112 **2.2. Aerodynamical characterization of the supersonic flows: Pitot tube measurements**

113   The uniformity of these parameters along the axis of the expansion was confirmed by

114 measuring the impact pressure, P_i, in the commonly named *Pitot tube* measurements, as a

115 function of the distance from the exit of the nozzle. The Pitot tube used in the continuous

116 mode consisted in a stainless steel tube (5 cm length) with an orifice of 2 mm, which was

117 connected to a 10 or 100 Torr pressure transducer. It was fixed on two manual translational

118 platforms for aligning the Pitot tube with the center of the gas flow. This system was

119 mounted on a motorized long-travel linear translational platform (Standa, 8MT195-740-

120 2.5).

121   As described in reference 30, the temperature, pressure and gas density of the jet

122   along the uniform supersonic flow were derived from the Mach number, M, which is

123   obtained from the average P_i obtained in the optimal length where the flow is uniform:

124
$$\frac{P_i}{P_{res}} = \left(\frac{(\gamma+1)M^2}{(\gamma-1)M^2+2} \right)^{\frac{\gamma}{\gamma-1}} \left(\frac{\gamma+1}{2\gamma M^2-\gamma+1} \right)^{\frac{1}{\gamma-1}}$$
(2)

125   The heat capacity ratio γ for the buffer gas and M values are shown in **Table 2**. In particular

126   for the gas mixture He/N$_2$, $\gamma_{mixture}$ was calculated considering the relationship between the

127   heat capacity of the gas mixture at constant pressure ($C_{p,mixture}$) and at constant volume

128   ($C_{v,mixture}$),

129                              $C_{p,mixture} = R + C_{v,mixture}$,   (3)

130   where $C_{v,mixture}$ includes the fraction of N$_2$ (60%) and He (40%) in the mixture. Therefore,

131     $\gamma_{mixture}$ can be expressed in terms of the individual C_v of the gases present in the mixture

132   ($C_{v,N_2} = 20.785$ J mol^{-1} K^{-1} and $C_{v,He} = 12.471$ J mol^{-1} K^{-1}):

133
$$\gamma_{mixture} = \frac{R}{0.6 \times C_{v,N_2} + 0.4 \times C_{v,He}} + 1$$
(4)

134   Temperature and gas densities were then obtained as described in reference 30. As an

135   example, **Fig 2** shows the spatial evolution of these two parameters for conditions **B** (see

136   **Figs S1** and **S2** of the supporting information for conditions **C** and **D** and reference 30 for

137   conditions **A**). As can be seen in the figures, the temperature and gas density of the jet are

138   uniform for several tens of centimeter from the exit of the nozzle, as well as it prolongs

139   three centimeters inside the divergent part of the nozzle. This length of uniformity is

140   sufficient to carry out the kinetic experiments in a timescale of several hundreds of

141   microseconds (hydrodynamic time, t_{hydro}, **Table 2**) and the methyl formate concentrations

142   used (see **Table 3**).

143

144   **2.3 PLP-LIF kinetic technique**

145   The conventional PLP-LIF technique has been widely employed in our laboratory for

146   kinetic studies on gas-phase reactions between OH radicals and atmospheric pollutants, as

147   previously described.[31,32] The OH radical was produced *in situ* by UV photolysis of H_2O_2

148   by a KrF excimer laser at 248 nm. The laser fluence measured by a calorimetric disk at the

149   exit of the Laval nozzle was *ca.* 1 mJ/(cm^2 pulse) for most of the experiments at 10 Hz. The

150   temporal evolution of $OH(X^2\Pi)$ was monitored by LIF at *ca.* 310 nm after excitation of OH

151   at *ca.* 282 nm using a frequency doubled dye laser (Lambda Physik, model Scanmate)

152   pumped by a XeCl excimer laser (Lambda Physik, model LPX105i). The LIF detection

153   arrangement consists of an optical system coupled with a filtered photomultiplier tube,

154   PMT. The band pass filter is centered at 310 nm with a full width at half maximum of 10

155   nm. The electrical signal from the PMT was transferred to a gated boxcar integration unit

156   and the integrated signal was recorded and processed into a computer by a home-made

157   LabView program.

158   OH radicals were lost mainly by reaction with methyl formate and at a lesser extent

159   by reaction with H_2O_2 (k_{prec}) and other processes such as diffusion of OH radicals out of the

160   detection zone and/or reaction with impurities, if present in the sample. As mentioned in

161   section 2.2, the timescale of the kinetic experiment was restricted by the uniformity of the

162   supersonic flow. For that reason, at all temperatures the maximum reaction time is the

163   hydrodynamic time, mentioned in **Table 2**. The reaction time during the kinetic

164   measurements was varied by changing the delay between the photolysis and the probe

165   lasers from *ca.* 20-40 μs before the trigger of the photolysis laser (to record the background

166   signal) to the hydrodynamic time.

167

168   **2.4 Chemicals**

169   He (99.999%, Praxair) and N_2 (99.999%, Praxair) were used as supplied. Liquid sample of

170   anhydrous $HC(O)OCH_3$ (99%, Sigma-Aldrich) was placed in a flask ($V = 250$ mL)

171   degassed by repeated freeze-pump-thaw cycles prior to its use. During the preparation of

172   diluted methyl formate in the buffer gas, the flask containing the liquid was introduced in a

173   beaker with water at room temperature to thermalize the sample, since there is a small gas

174   expansion and, consequently, temperature and vapor pressure of the methyl formate

175   decrease. Aqueous solution of H_2O_2 (Sharlab, initially at 50% w/v) was pre-concentrated as

176   described earlier.[31,32]

177

178   **3 Results and Discussion**

179   **3.1. Determination of $k_{OH}(T)$**

180   The kinetic study of reaction (1) was performed under *pseudo*-first order conditions

181   ($[OH]_0 \ll [HC(O)OCH_3]$ and $[H_2O_2]$). $[HC(O)OCH_3]$ concentration was calculated from the

182   dilution factors, the mass flow rates, and T and P of the jet. Concentration ranges used in

183   the kinetic analysis are shown in **Table 3**. In order to check that the *pseudo*-first order

184   conditions were accomplished, the gas-phase concentration of H_2O_2 in the jet was optically

185   measured before entering the reservoir (at room temperature) by UV spectroscopy at 254

186   nm using a gas cell with a path length of 108 cm. After correction of temperature and

187   pressure (for conditions **D**), $[H_2O_2]$ in the jet was found to be lower than 10^{13} cm^{-3} in this

188   case. Accurate calculation of $[OH]_0$ would require the knowledge of absorption cross

189   section of H_2O_2 at 248 nm and the OH quantum yield at lower temperatures than 298 K.

190   Nicovich and Wine[33] measured the temperature dependence of σ_λ for 230 nm $\leq \lambda \leq$ 295 nm

191   between 285 and 381 K. No appreciable change was observed in σ_λ in this wavelength

192   range. In any case, at the photolysis laser fluence used and considering the absorption cross

193   section of H_2O_2 and quantum yield of OH at room temperature,[34] the initial OH

194   concentration between 22 K and 64 K is expected to be several orders of magnitude lower

195   (below 10^{10} cm^{-3}) than that of its precursor. Consequently, the *pseudo*-first order conditions

196   are achieved at all reagent concentrations.

197   In the absence of OH-precursor, Le Calvé *et al.*[26] detected a fluorescence emission

198   at 310 nm attributed to CH_3O radicals formed in the photolysis of methyl formate, (1.94-

199   6.85)$\times 10^{15}$ cm^{-3}, at 248 nm. In the present work, nonetheless, no emission was observed in

200   the photolysis of methyl formate at 248 nm in the absence of H_2O_2 at the concentrations

201   and laser fluences employed. Therefore, the recorded LIF temporal profiles correspond

202   exclusively to OH radicals. **Fig 3** shows an example of the temporal evolution of OH

203   radicals in the presence of methyl formate recorded at 43 K. The temporal profiles of the

204   OH LIF signal (I_{LIF}) were analyzed after 20-40 μs depending on the methyl formate

205   concentration, because some rotational relaxation occurs at shorter times. At all

206   temperatures of the jet, I_{LIF} did not fully decay in the available timescale at the methyl

207   formate concentrations, which had to be low enough to avoid secondary chemistry (as

208   discussed below).

209   Under these conditions and after rotational relaxation of OH, the non-linear least

210   square fit of the LIF data to a single exponential function (solid line in **Fig 3**) yields the

211   pseudo-first order rate coefficient, k', for a fixed concentration of methyl formate (and

212   H_2O_2):

213                         $k' = k_{OH}(T)[HC(O)OCH_3] + k_0$ (5)

214   where k_0 (= $k_{prec}(T)[H_2O_2] + k_{other\ losses}$) is the *pseudo*-first order coefficient obtained in the

215   absence of $HC(O)OCH_3$. During a kinetic experiment at a single temperature, $[H_2O_2]$ was

216   kept constant. Averaged k_0 (in s^{-1}) were 6400 at 22 K, 3700 at 43 K, 2100 at 52 K and 5100

217   at 64 K. Individual $k_{OH}(T)$ were obtained from the slope of the plots of the *pseudo*-first

218   order rate coefficients k' corrected by k_0 against the $HC(O)OCH_3$ concentrations.

219                         $k' - k_0 = k_{OH}(T)[HC(O)OCH_3]$ (6)

220   All obtained $k'-k_0$ are plotted as a function of reactant concentration in **Fig 4** for all

221   experiments carried out. As it can be seen in **Fig 4.a**, at 22 K a curvature in the plot of $k'-k_0$

222   versus $[HC(O)OCH_3]$ was observed above 3×10^{13} cm^{-3}, indicating that an additional loss of

223   methyl formate is occurring by complexing formation in the ultracold jet (T=22 K). This

224   effect was also observed in the reaction of OH with 1-butene at 22 K.[30] For that reason the

225   kinetic analysis was constrained to the range of $[HC(O)OCH_3]$ where *pseudo*-first order

226   plots were linear. As can be seen in **Table 3** and **Fig 4**, higher concentrations of

227    $HC(O)OCH_3$ could be accessible at higher temperatures, because the formation of

228   aggregates is kinetically less efficient at the total gas density of these experiments with

229   respect to 22 K.

230

231   **3.2. Temperature Dependence of $k_{OH}(T)$: Enhancement at ultra-low temperatures**

232   $k_{OH}(T)$ values obtained are listed in **Table 3** and depicted in **Fig 5**. As it can be seen, the

233   reactivity of $HC(O)OCH_3$ toward OH radicals is high in the investigated temperature range,

234   decreasing rapidly from 22 to 64 K. In **Table 3**, the enhancement factor relative to

235   $k_{OH}(64K)$ is also shown for all temperatures. The observed enhancement of $k_{OH}(T)$ over 40

236   K in the T-range of interest in the ISM is of one order of magnitude. The enhancement

237   factor is *ca.* 4 and 2 at 43 and 52 K, respectively.

238   The observed temperature dependence of $k_{OH}(T)$ between 22 and 64 K was first fitted

239   to the following expression commonly used in kinetic databases employed in astrophysical

240   models:[35]

241                        $$k_{OH}(T) = \alpha \ (T/ 300 \ K)^{\beta} \exp(-\gamma/ T) \qquad\qquad (7)$$

242   The fit to this three-parameter expression yielded a $\gamma \sim 0$ K. Therefore, we deliberately

243   fixed this parameter to 0 K without affecting significantly the accuracy of the fit. As $\beta<0$

244   (see **Fig 5**), extrapolation of Eq.(7) to temperatures close to absolute zero ($T<22$ K)

245   provides however unrealistic results ($T \rightarrow 0$ K, $k_{OH}(T) \rightarrow \infty$). Interestingly, a single

246   exponential expression of the form,

247                        $$k_{OH}(T) = a \exp(- b \times T), \qquad\qquad (8)$$

248   describes perfectly the observed T-dependence of $k_{OH}(T)$ in the investigated range. The

249   resulting parameters a and b are given in **Fig 5**. Note that even though Eq.(8) has no

250   physical meaning, it predicts a reasonable k_{OH} at 10 K (2.38×10^{-10} cm^3 s^{-1}) and at 0 K

251   (3.84×10^{-10} cm^3 s^{-1}). Of course, the "real" kinetic behavior may be different as that

252   predicted, hence Eq.(8) should be exclusively used for the temperature range 22-64 K.

253   As shown in **Table 4** and **Fig 6**, the trend in the temperature dependence of $k_{OH}(T)$

254   is noticeably different at $T<64$ K (of interest in the ISM, this work), between 233 and 372 K

12

255   (of interest in terrestrial atmosphere) [23-27,29] and at higher temperatures (of interest in

256   combustion chemistry).[27,28] At room temperature, Wallington *et al.*[23], Good *et al.* [24] and

257   Szilagyi *et al.* [25] reported experimental rate coefficients $k_{OH}(T)$ in quite good agreement

258   with each other. The typical measured value was about 2×10^{-13} cm^3s^{-1}. Le Calvé *et al.*[26]

259   extended the kinetic study of reaction (1) to temperatures between 233 and 372 K. These

260   authors observed a small positive temperature dependence with an activation energy of *ca.*

261   1 kcal/mol. At temperatures of interest in combustion chemistry, Lam *et al.*[27]

262   experimentally reported a much stronger temperature dependence with activation energy of

263   4 kcal/mol between 880 and 1337 K.

264   From a theoretical point of view, a few works can be found in the literature. In 1999

265   Good *et al.*[24] used *ab initio* molecular orbital theory to calculate the rate coefficient at 298

266   K obtaining a value of 1.88×10^{-13} cm^3s^{-1}, in excellent agreement with their experimental

267   contribution and other studies. The rate coefficient was calculated by transition state theory

268   (TST) taking into account the Wigner correction accounting for the effect of tunneling.

269   More recently, Tan *et al.*[28] performed *ab initio* calculations in the temperature range 300-

270   1500 K, and found that $k_{OH}(300K) \sim 8\times10^{-15}$ cm^3s^{-1} which is lower, by more than one order

271   of magnitude, than the experimental ones. TST in conjunction with the CANTHERM code

272   was used by Tan *et al.*[28] to calculate these rate coefficients and the Eckart correction was

273   applied to take into account tunneling. A third study was provided by Elm *et al.*[29] The

274   originality of their work was to calculate the rate coefficient at 298 K and 1 atm for several

275   functionals and tunneling corrections using the conventional TST. They concluded that

276   BH&HLYP and MP2 functionals were those leading to the best agreement with

277   experiments, provided that the tunneling Bell correction was used. Interestingly, the rate

278   coefficient was increased by a factor of 36 (BH&HLYP) or 90 (MP2) when the Bell

279   correction was applied to their UCCSD(T)-F12a single point corrected k_{OH}(298K)

280   indicating the very large effect of tunneling in this reaction.

281   To our knowledge, no attempt has been undertaken to determine rate coefficients at

282   sub-ambient temperatures using these theoretical methods. As it can be seen in **Fig 6**, an

283   increase of roughly three orders of magnitude for $k_{OH}(T)$ is observed between 298 K and 22

284   K, whereas the rate coefficient shows a classical Arrhenius increase at higher

285   temperatures.[27] This kind of behavior has been seen for the first time only very recently for

286   other oxygenated compounds[36-40] reacting with OH. This spectacular change in k_{OH} could

287   be explained by a change in the mechanism driving the dynamics of the reaction comparing

288   to the suprathermal domain.

289

290   **3.3. Reaction mechanisms and products**

291   The reaction pathways of the OH + $CH_3C(O)OH$ reaction have been investigated by

292   Good *et al.*[24] and more extensively by Tan *et al.*[28]. In the latter study, the authors found that

293   the reaction proceeds through H abstraction at either the methyl group or the formyl group

294   of methyl formate, leading to the exothermic formation of $CH_2C(O)OH$ + H_2O or

295    $CH_3C(O)O$ + H_2O, respectively. Four reaction pathways were identified, all starting with

296   the reversible formation of a weakly bound pre-reactive complex followed by an

297   irreversible reaction through a transition state to the above mentioned products. As two pre-

298   reactive complexes have been found to stand in a very shallow well (~1 kcal/mol), only

299   those channels passing through the deeper wells (3.7 and 3.4 kcal/mol, respectively) have

300   been considered by the authors. The barrier heights for the two corresponding transition

301   states were 3.5 and 4.0 kcal/mol respectively. This situation is qualitatively similar to that

302   observed for the reaction of OH with methanol[37,39], acetone[36,38] and dimethyl ether[36,38] and

303   can qualitatively explain our observations. The pre-reactive complexes are expected to be

304   short-lived at "high" temperatures with the propensity to break back to the reactants,

305   whereas the activation barrier to the transition state leads to a standard Arrhenius behavior.

306   At lower temperatures, the pre-reactive complex lifetime should raise giving a chance to the

307   rate coefficient to increase significantly either by adduct stabilization (three body process)

308   or tunneling through products (binary process). Although the present experimental study

309   cannot discriminate from these two options, the theoretical work carried out by Elm *et al.*[29]

310   showed that tunneling has a major contribution, at least at 298 K. This should be even

311   stronger at lower temperatures. Note that terms such as "high" and "low" are presently quite

312   vague, because there is no sufficient data available to identify the temperature at which the

313   rate coefficient would reach its minimum value. Further experimental and theoretical works

314   are evidently needed to make these aspects clearer.

315

316   **3.4. Branching ratios**

317   Another aspect to consider is the potential organic radical formation in reaction (1).

318   Quantitative information concerning the products of reaction (1) cannot be derived from the

319   present experiments, nevertheless some comments are worthwhile. As mentioned earlier, in

320   the titled reaction, hydrogen atom abstraction by OH radicals can occur at either the formyl

321   group (channel 1a) or the methyl group (channel 1b):

322                    $OH + HC(O)OCH_3 \rightarrow C(O)OCH_3 + H_2O$ (1a)

323                    $\rightarrow HC(O)OCH_2 + H_2O$ (1b)

15

324   At 298 K, Le Calvé et al.[24] predicted, based on structure-activity (SAR) calculations that

325   both channels accounted for *ca.* 50% of the overall rate coefficient k_{OH}. From *ab initio*

326   calculations, the predicted branching ratio k_{1a}/k_{1b} at room temperature greatly differs. Good

327   *et al.*[25] reported that that formation of $C(O)OCH_3$ radicals (channel 1a) was the major

328   reaction pathway, accounting for 86%, while Tan *et al.*[28] predicted that formation of

329    $HC(O)OCH_2$ radicals (channel 1b) was the major reaction pathway, accounting for 66% of

330   k_{OH}. At higher temperatures (*e.g.* 1168 K), Lam *et al.*[27] estimated that channel (1b) is the

331   main reaction pathway accounting for 68% of overall k_{OH}, which is lower than that derived

332   from *ab initio* calculations by Tan *et al.*[28] (*ca.* 54% for channel 1b). In light of these

333   discrepant results and given that the formation of $C(O)OCH_3$ and $HC(O)OCH_2$ radicals is

334   not quantitatively known, we cannot assert which channel could become more important at

335   lower temperatures than 298 K. However, by comparison with the reaction of OH with

336   CH_3OH, it could be expected a change in the yield of the reaction products at low

337   temperatures with respect to that found at room temperature.[37] According to master

338   equation calculations carried out by Shannon *et al.*, the H-atom abstraction by OH radicals

339   seems to exclusively occur at low temperatures from the –OH group of methanol.[37] These

340   calculations show that the branching ratio for the $CH_3O + H_2O$ channel reaches unity at

341   temperatures lower than 70 K. In contrast, at room temperature the main reaction product is

342   CH_2OH radical formed through the H-abstraction from methyl group of methanol.[41] Further

343   mechanistic studies on reaction (1), especially at low temperatures are indispensable to

344   check if the $C(O)OCH_3$ radical can be the main reaction product at temperatures of the

345   ISM.

346

347 **4. Conclusions and astrophysical impact**

348 The present work constitutes the first determination of the rate coefficients for the gas-

349 phase reaction of methyl formate and OH radicals at ultra-low temperatures. Our results

350 show that, at extremely low temperatures, the investigated reaction (1) is a very efficient

351 loss route for $HC(O)OCH_3$ in the gas phase, up to three orders of magnitude faster than at

352 room temperature. Acharyya et al.[42] have recently evidenced the importance of determining

353 gas-phase rate coefficients at temperatures found in ISM molecular clouds (close to 10 K)

354 for the reaction of OH with methanol. The acceleration of k_{OH} for this reaction has a

355 marked influence on the modeled abundances of CH_3O radicals. For that reason, the

356 inclusion of our results on the OH+methyl formate in astrochemical models may have a

357 great impact and would help to improve/shed light on the interpretation of the detected

358 abundances of methyl formate in the various environments of the ISM. These

359 measurements can also stimulate attempts to detect the radicals issued from the studied

360 reaction, which have not been looked for until now.

361 The temperature dependence of reaction (1) has been found to be similar to that

362 observed for other oxygenated species reacting with OH[35-39]. With the exception of the

363 reaction of OH with methanol, Shannon et al.[37] and Caravan et al.[39] reported that a pressure

364 dependence of $k_{OH}(T)$ was observed at gas densities between 3.2×10^{16} and 2.6×10^{17} cm^{-3} in

365 the temperature range ca. 88 and 140 K[37,39]. Despite the present work cannot provide any

366 evidence of a pressure dependence of the rate coefficient k_{OH}, this will be explored in the

367 near future with specific Laval nozzles, operating at different gas densities for a same

368 temperature.

369   Further CRESU experiments are also needed at different temperatures to have a

370   complete picture of the kinetic behavior of reaction (1) at sub-ambient temperatures. For

371   this purpose, new Laval nozzles will be constructed in our laboratory to probe temperatures

372   below 20 K and above 64 K.

373

374

384   **References**

385   1   S. Weinreb, A. H. Barrett, M. L. Meeks, J. C. Henry, Radio observations of OH in
386   the interstellar medium. *Nature*, 1963, **200**, 829.

387   2   R. D. Brown, J. G. Crofts, P. D. Godfrey, F. F. Gardner, B. J. Robinson, J. B.
388   Whiteoak, Discovery of interstellar methyl formate. *Astrophys J.* 1975**, 197**, L29.

389   3   E. Churchwell, G. Winnewisser, Observations of methyl formate in the galactic
390   center *Astron. Astrophys.* 1975, **45**, 229.

391   4   E. C. Sutton, R. Peng, W. C. Danchi, P. A. Jaminet, G. Sandell, A. P. G. Russell,
392   The distribution of molecules in the core of OMC-1. *Astrophys. J.* 1995, **97**, 455.

393   5   B. Tercero, L. Margulès, M. Carvajal, R.A. Motiyenko, T.R. Huet, E.A. Alekseev, I.
394   Kleiner, J.C. Guillemin, H. Møllendal, J. Cernicharo. Microwave and submillieter
395   spectroscopy and first ISA detection of ^{18}O-methyl formate. *Astron. Astrophys.*
396   2012, **538**, A119-1.

397   6   S. Cazaux, A. G. G. M. Tielens, C. Ceccarelli, A. Castets, V. Wakelam, E. Caux, B.
398   Parise, D.Teyssier, The Hot Core around the low-mass protostar IRAS 16293-2422:
399   Scoundrels Rule! *Astrophys. J. Lett.* 2003, **593**, L51.

400   7   S. Bottinelli, C. Ceccarelli, B. Lefloch, J. P. Williams, A. Castets, E. Caux, S.
401   Cazaux, S. Maret, B. Parise, A. G. G. M. Tielens, Complex molecules in the hot
402   core of the low-mass protostar NGC 1333 IRAS 4A. *Astrophys. J.* 2004, **615**, 354.

403   8   A.J. Remijan, J. M. Hollis, IRAS 16293-2422: Evidence for infall onto a
404   counterrotating protostellar accretion disk. *Astrophys. J.* 2006, **640**, 842.

405   9   K.I. Öberg, S. Bottinelli, J.K. Jorgensen, E.F.van Dishoeck, A cold complex
406   chemistry toward the low-mass protostar B1-b: Evidence for complex molecule
407   production in ices. *Astrophys. J.* 2010, **761**, 825.

408   10   A.A. Jaber, C. Ceccarelli, C. Kahane, E. Caux, The census of complex organic
409   molecules in the solar-type protostar IRAS16293-2422. *Astrophys. J.* 2014, **791**, 29.

410   11   A. Bacmann, V. Taquet, A. Faure, C. Kahane, C. Ceccarelli, Detection of complex
411   organic molecules in a prestellar core: a new challenge for astrochemical models.
412   *Astron. Astrophys.* 2012, **541**, L12-1.

413   12   A. Horn, H. Møllendal, O. Sekiguchi, E. Uggerud, H. Roberts, E. Herbst, A.A.
414   Viggiano, T.D. Fridgen, The gas-phase formation of methyl formate in hot
415   molecular cores. *Astrophys J.*, 2004, **611**, 605.

416   13   R.T. Garrod, E. Herbst, Formation of methyl formate and other organic species in
417   the warm-up phase of hot molecular cores. *Astron. Astrophys.* 2006, **457**, 927.

418   14   R.T. Garrod, S.L.W. Weaver, E. Herbst, Complex chemistry in star-forming
419   regions: an expanded gas-grain warm-up chemical model. *Astrophys. J.* 2008, **682**,
420   283.

421   15   C.J. Bennett, R.I. Kaiser, On the formation of glycolaldehyde (HCOCH$_2$OH) and
422   methyl formate (HCOOCH$_3$) in interstellar ice analogs. *Astrophys. J.* 2007, **661**,
423   899.

424   16   J. C. Laas, R.T. Garrod, E. Herbst, S.L.W. Weaver, Contributions from grain
425   surface and gas phase chemistry to the formation of methyl formate and its
426   structural isomers. *Astrophys. J.,* 2011, **728**, 71.

427   17   C.A. Cole, N. Wehres, Z. Yang, D.L. Thomsen, T.P. Snow, V.M. Bierbaum, A Gas-
428   phase formation route to interstellar trans-methyl formate. *Astrophys. J. Lett.* 2012,
429   **754**, L5-1.

430   18   N. Balucani, C. Ceccarelli, V.Taquet, Formation of complex organic molecules in
431   cold objects: the role of gas phase reactions. *Mon. Not. R. Astron. Soc*. 2015, **449**,
432   L16.

433   19   P. Modica, M.E. Palumbo, Formation of methyl formate after cosmic ion irradiation
434   of icy grain mantless. *Astron. Astrophys*. 2010, **519**, A22-1.

435   20   S-H. Lee, Photodissociation dynamics of methyl formate at 193.3 nm: Branching
436   ratios, kinetic-energy distribution, and angular anisotropies of products. *J. Chem.*
437   *Phys.* 2008, **129**, 194304.

438   21   M-H. Chao, P-Y. Tsai, K-C. Lin, Molecular elimination of methyl formate in
439   photolysis at 234 nm: roaming vs. transition state-type mechanism. *Phys. Chem.*
440   *Chem. Phys.* 2011, **13**, 7154.

441   22   P-Y. Tsai, M-H. Chao, T. Kasai, K-C. Lin, A. Lombardi, F. Palazzetti, V. Aquilanti,
442   Roads leading to roam. Role of triplet fragmentation and of conical intersections in
443   photochemical reactions: experiments and theory on methyl formate, *Phys. Chem.*
444   *Chem. Phys.* 2014, **16**, 2854.

445   23   T.J. Wallington, P. Dagaut, R. Liu, M.J. Kurylo, The gas phase reactions of
446   hydroxyl radicals with a series of esters over the temperature range 240-440 K. *Int.*
447   *J. Chem. Kinet.* 1988, **20**, 177.

448   24   D.A. Good, J. Hanson, J.S. Francisco, Z. Li, G-R. Jeong. Kinetics and reaction
449   mechanism of hydroxyl radical reaction with methyl formate. *J. Phys. Chem. A*
450   1999, **103**, 10893.

451   25   I. Szilágyi, S. Dóbé, T. Bérces, F. Márta, B. Viskolcz, Direct kinetic study of
452   reactions of hydroxyl radicals with alkyl formats. *Z. Phys. Chem*. 2004, **218**, 479.

453   26   S. Le Calvé, G. Le Bras, A. Mellouki, Temperature dependence for the rate
454   coefficients of the reactions of the OH radical with a series of formates. *J. Phys.*
455   *Chem. A.* 1997, **101**, 5489.

456   27   K.Y. Lam, D.F. Davidson, R.K. Hanson, High-temperature measurements of the
457   reactions of OH with small methyl esters: methyl formate, methyl acetate, methyl
458   propanoate, and methyl butanoate. *J. Phys. Chem. A* 2012, **116**, 12229.

459   28   T. Tan, M. Pavone, D.B. Krisiloff, E.A. Carter, Ab initio reaction kinetics of
460   hydrogen abstraction from methyl formate by hydrogen, methyl, oxygen, hydroxyl,
461   and hydroperoxy radicals. *J. Phys. Chem. A*. 2012, **116**, 8431.

462   29 J. Elm, S. Jørgensen, M. Bilde, K.V. Mikkelsen, Ambient reaction kinetics of
463   atmospheric oxygenated organics with the OH radical: a computational
464   methodology study. *Phys. Chem. Chem. Phys.*, 2013, **15**, 9636.

465   30 E. Jiménez, B. Ballesteros, A. Canosa, T. M. Townsend, F.J. Maigler, V. Napal, B.
466   R. Rowe, J. Albaladejo, Development of a pulsed uniform supersonic gas expansion
467   system based on an aerodynamic chopper for gas phase reaction kinetic studies at
468   ultra-low temperatures. *Rev. Sci. Instrum.* 2015, **86**, 045108-1.

469   31 E. Jiménez, B. Ballesteros, E. Martínez, J. Albaladejo, Tropospheric reaction of OH
470   with selected linear ketones: kinetic studies between 228 and 405 K. *Environ. Sci.
471   Technol.* 2005, **39**, 814.

472   32 E. Jiménez, B. Lanza, A. Garzón, B. Ballesteros, J. Albaladejo, Atmospheric
473   degradation of 2-butanol, and some branched alcohols 2-methyl-2-butanol, and 2,3-
474   dimethyl-2-butanol: OH kinetics and UV absorption cross sections. *J. Phys. Chem.
475   A* 2005, **109**, 10903.

476   33 J. M. Nicovich, P. H. Wine, Temperature-dependent absorption cross sections for
477   hydrogen peroxide vapor. *J. Geophys. Res.,* 1988, **93**, 2417.

478   34 S. P. Sander, J. Abbatt, J. R. Barker, J. B. Burkholder, R. R. Friedl, D. M. Golden,
479   R. E. Huie, C. E. Kolb, M. J. Kurylo, G. K. Moortgat, V. L. Orkin and P. H. Wine
480   "Chemical Kinetics and Photochemical Data for Use in Atmospheric Studies,
481   Evaluation No. 17," JPL Publication 10-6, Jet Propulsion Laboratory, Pasadena,
482   2011 http://jpldataeval.jpl.nasa.gov

483   35 D. McElroy, C. Walsh, A.J. Markwick, M.A. Cordiner, K. Smith, and T.J. Millar.
484   The UMIST database for astrochemistry 2012. *Astron. Astrophys.*, 2013, **550**, A36.

485   36 R.J. Shannon, S. Taylor, A. Goddard, M.A. Blitz, D.E. Heard, Observation of a
486   large negative temperature dependence for rate coefficients of reactions of OH with
487   oxygenated volatile organic compounds studied at 86-112 K. *Phys. Chem. Chem.
488   Phys.* 2010, **12**, 13511.

489   37 R.J. Shannon, M.A. Blitz, A. Goddard, D.E. Heard, Accelerated chemistry in the
490   reaction between the hydroxyl radical and methanol at interstellar temperatures
491   facilitated by tunneling. *Nature Chem.,* 2013, **5**, 745.

492   38 R.J. Shannon, R.L. Caravan, M.A. Blitz, D.E. Heard, A combined experimental and
493   theoretical study of reactions between the hydroxyl radical and oxygenated
494   hydrocarbons relevant to astrochemical environments, *Phys. Chem. Chem. Phys.,*
495   2014, **16**, 3466.

496   39 J.C. Gómez Martín, R.L. Caravan, M.A. Blitz, D.E. Heard, J.M.C. Plane, Low
497   Temperature Kinetics of the CH_3OH + OH Reaction, *J. Phys. Chem. A* 2014, **118**,
498   2693.

499   40 R.L. Caravan, R.J. Shannon, T. Lewis, M.A. Blitz, D.E. Heard, Measurements of
500   rate coefficients for reactions of OH with ethanol and propan-2-ol at very low
501   temperatures. *J. Phys. Chem. A* 2015, **119**, 7130.

502 41 E. Jiménez, M.K. Gilles, A. R. Ravishankara, Kinetics of the reactions of hydroxyl
503   radical with CH_3OH and C_2H_5OH between 235 and 360 K. *J. Photochem.*
504   *Photobiol. A*, 2003, **157**, 237.

505 42 K. Acharyya, E. Herbst, R. L. Caravan, R. J. Shannon, M. A. Blitz, DE Heard, The
506   importance of OH radical–neutral low temperature tunnelling reactions in
507   interstellar clouds using a new model. *Molec. Phys*. 2015, **113**, 2243.

508

509   **Figures**

510
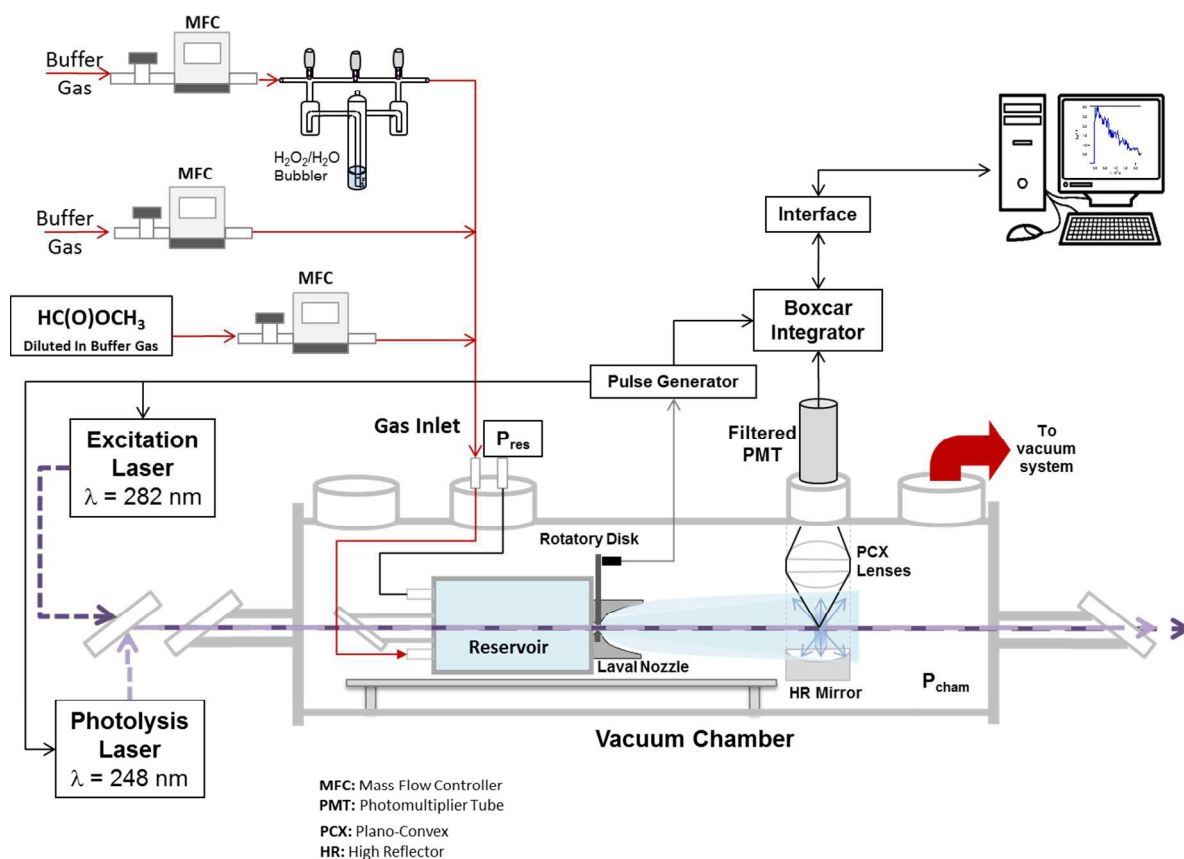
511
512   **Fig 1.** Schematics of the experimental system employed: CRESU apparatus coupled to
513   PLP-LIF.

514

a)

$T_{avg} = (42.5 \pm 1.3)$ K

b)

$n_{avg} = (5.22 \pm 0.33) \times 10^{16}$ cm^{-3}
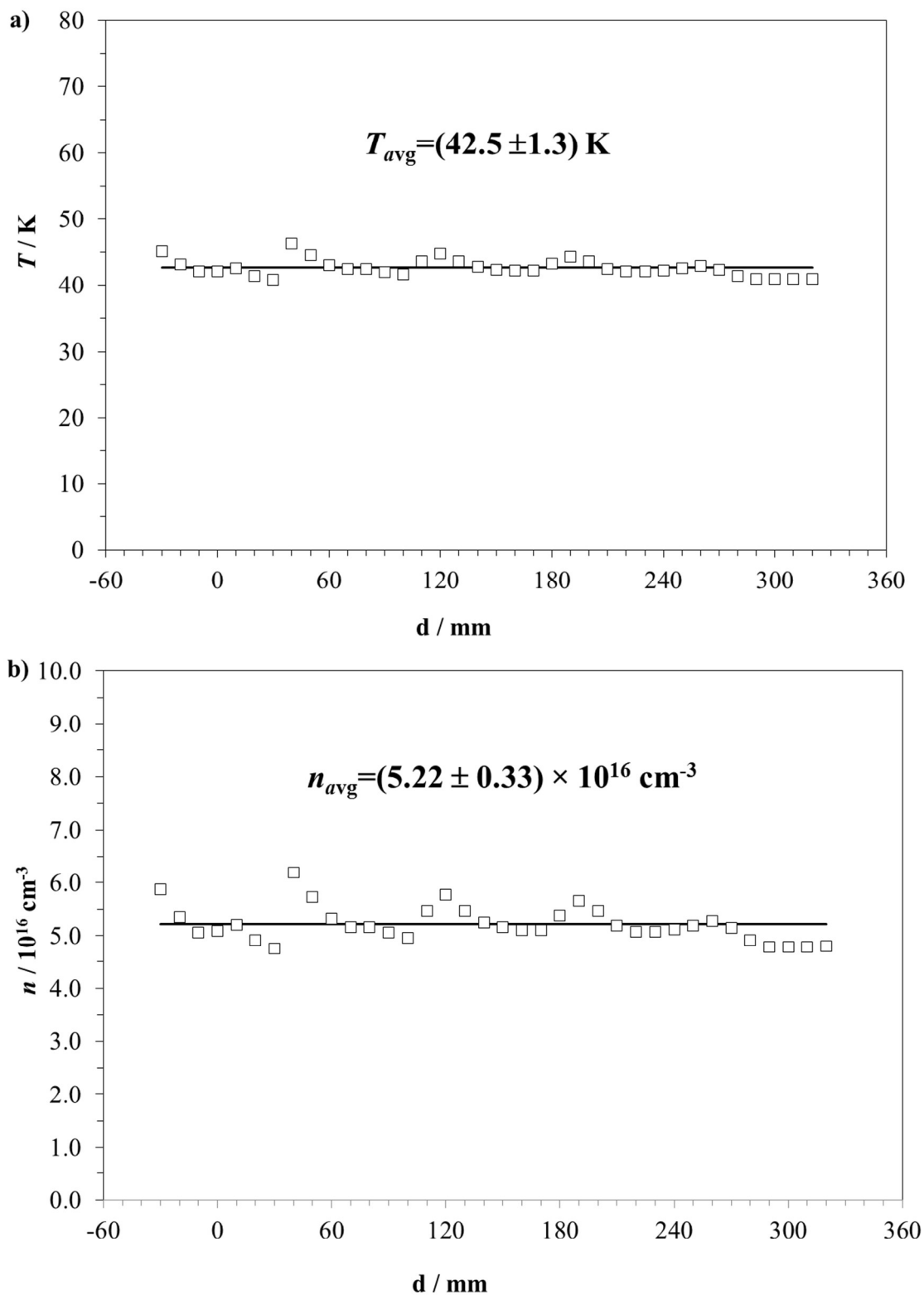
515

516   **Fig 2.** Spatial profiles of the temperature and total gas density of the jet for experimental
517   conditions **B**. Uncertainty is $\pm\sigma$.

518
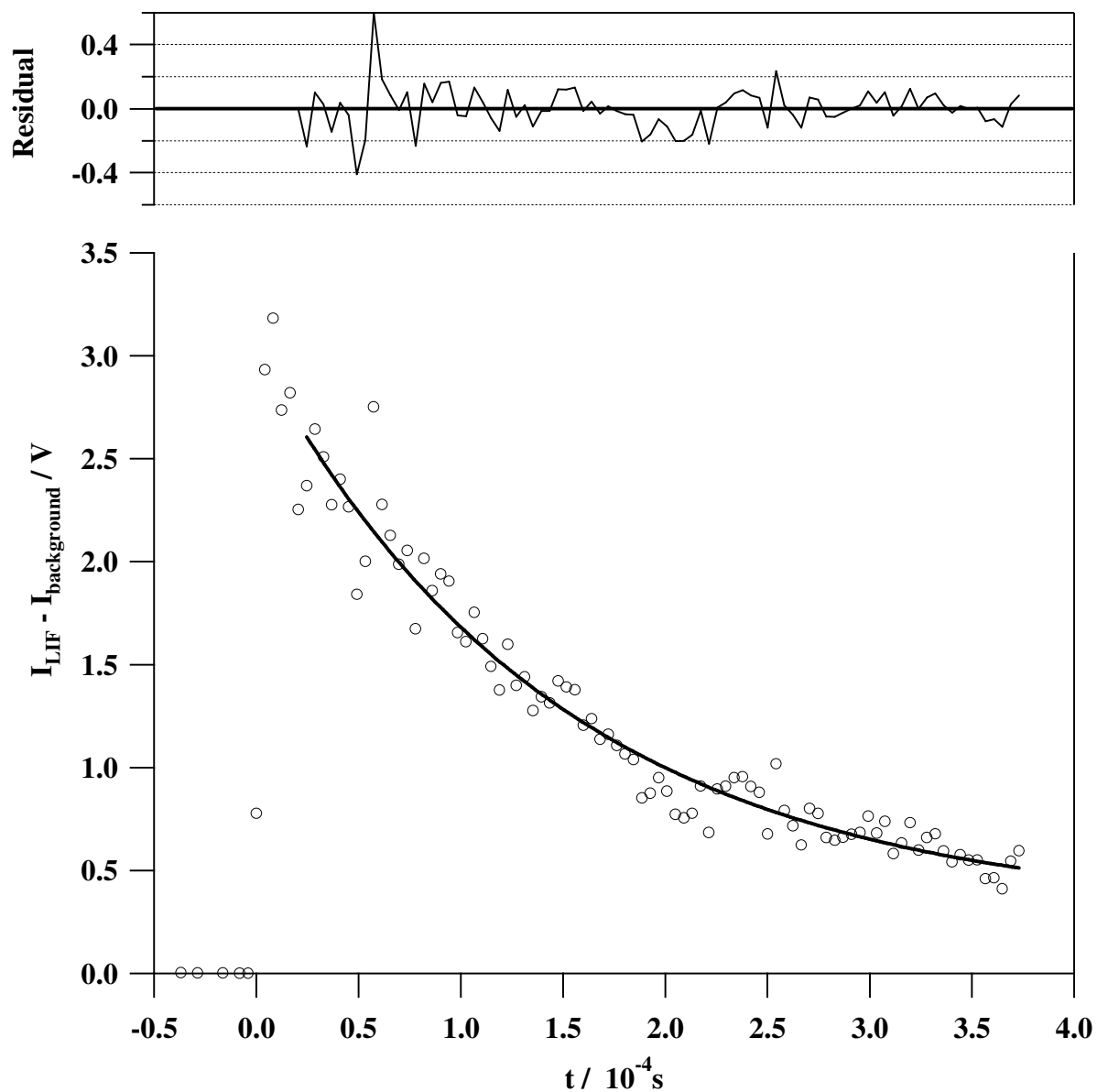
Fig 3. Example of a temporal profile of the LIF signal from OH radicals recorded at $T = 43$ K in the presence of methyl formate (1.86×10^{13} cm^{-3}). The fit started at 20 μs to ensure fully rotational relaxation of OH.
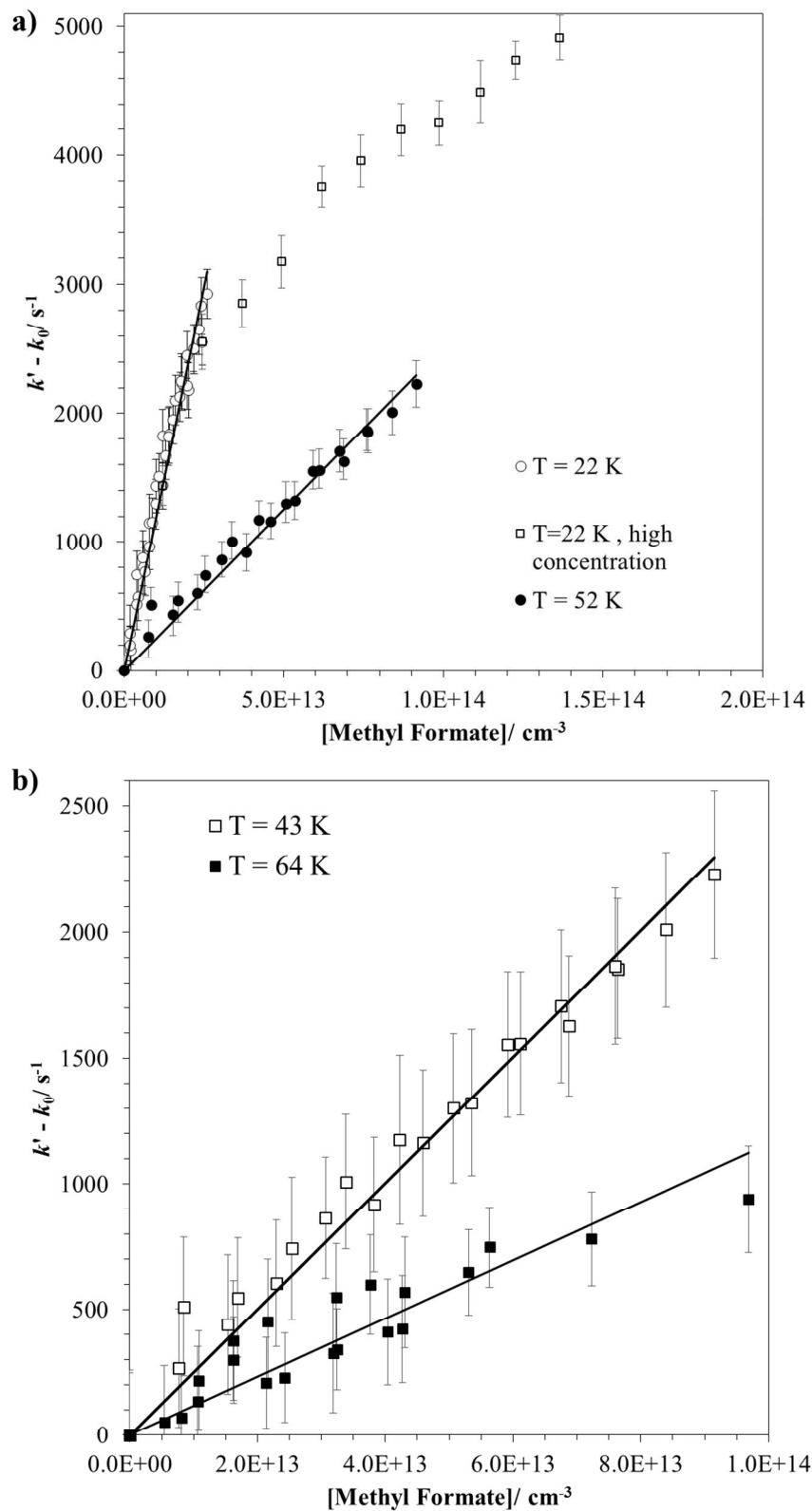
Fig 4. Plots of corrected *pseudo*-first order rate coefficient *versus* methyl formate concentration.

27
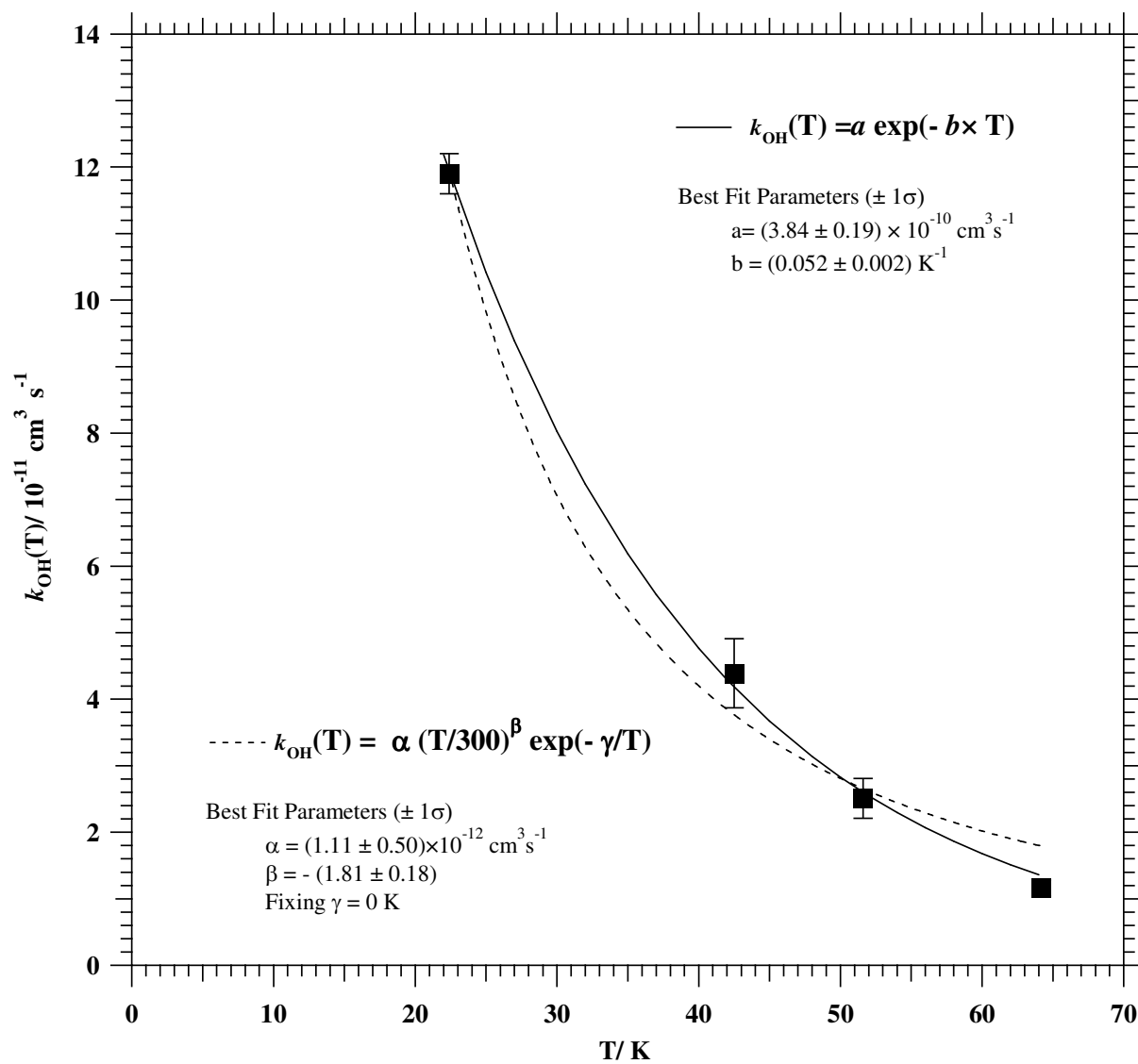
Fig 5. Temperature dependence of $k_{OH}(T)$ for the reaction of OH with methyl formate between 22 and 64 K.
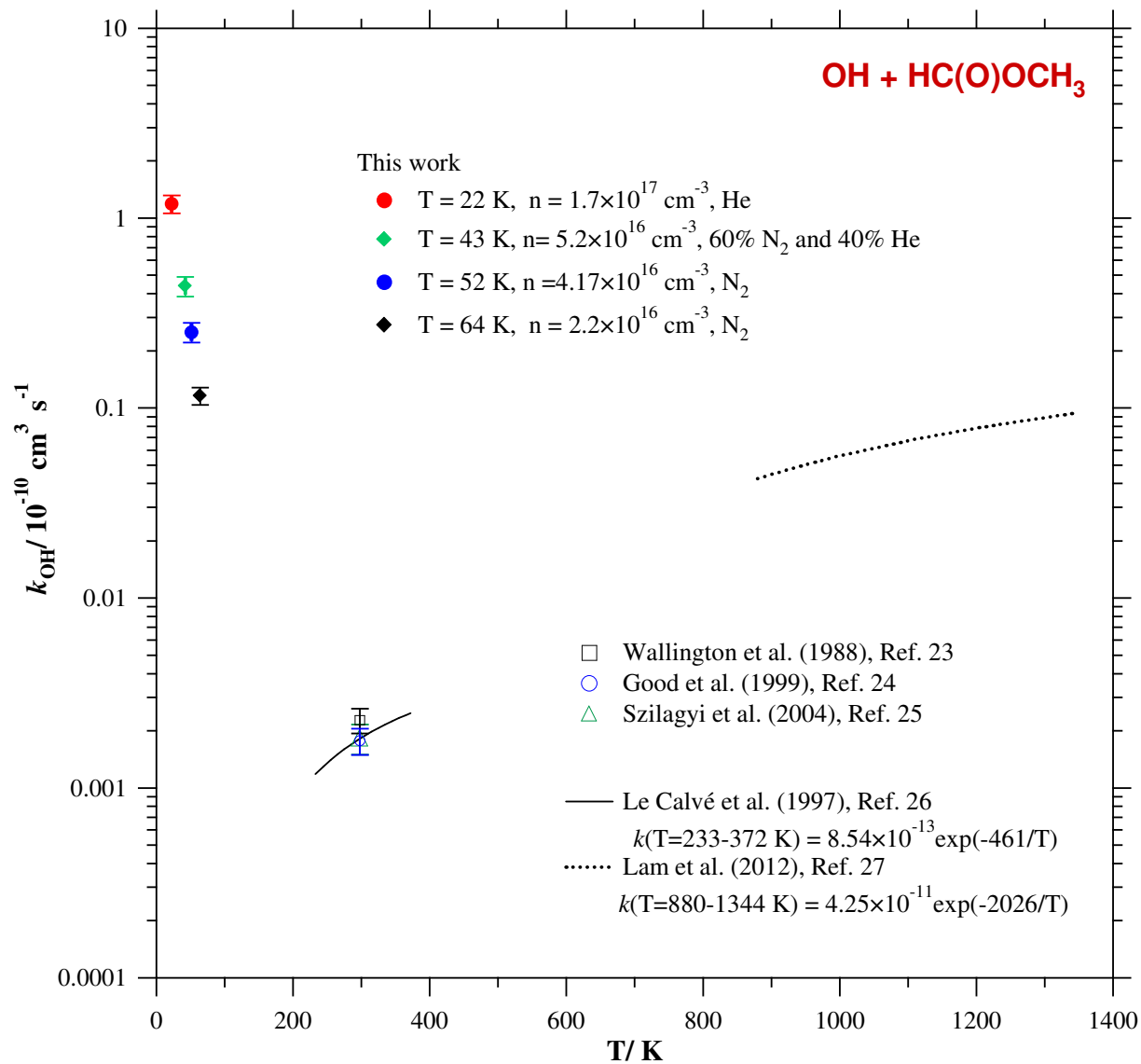
Fig 6. Temperature dependence of $k_{OH}(T)$ for the investigated reaction (1) between 22 and 1344 K.

Physical Chemistry Chemical Physics **Page 30 of 33**

Tables

Table 1. Summary of the experimental conditions employed in this work (T_{res} = 297±1 K).

Conditions	Gas Flow	Buffer Gas (%)	F_{He}/ slpm	F_{N_2}/ slpm	F_{buffer}/ slpm	$F_{H_2O_2}$*/ sccm	F_R/ sccm	$f \times 10^{-3}$	P_{res}/ mbar	P_{cham}/ mbar
A	Pulsed	He (100%)	8.4	0	8.4	95-190	48-592	1.9-12	337.0	0.621
B	Continuous	N$_2$ (60%)	6.0	9.0	15.0	190	45-550	37-77	127.1	0.296
		He (40%)								
C	Continuous	N$_2$ (100%)	0	12.6	12.6	190	47-562	50-55	136.2	0.279
D	Continuous	N$_2$ (100%)	0	4.4	4.4	47	48-573	19-38	41.67	0.183

* Flow of buffer gas through the bubbler containing the aqueous solution of OH precursor; F_R is the flow rate of the diluted methyl formate through the reservoir; f is the dilution factor of the methyl formate in the storage bulb.

Table 2. Characteristics of the gas flows: average impact pressure (P_i), heat capacity ratio (γ), Mach number (M), temperature of the jet (T), hydrodynamic time (t_{hydro}) and the length of the flow uniformity (d).

Conditions	P_i /mbar	γ	M	T/ K	t_{hydro}/ μs	d/ cm
A	29.1±2.6	1.6667	6.1±0.2	22.4 ±1.4	244	40
B	10.5±0.6	1.4762	5.0±0.1	42.5±1.3	414	32
C	9.3±0.7	1.4000	4.9±0.1	51.6±1.7	777	52
D	4.7±0.3	1.4000	4.2±0.1	64.2±1.7	202	11

Table 3. Rate coefficients for the gas-phase reaction of OH with methyl formate between 22 and 64 K and enhancement factors with respect to k_{OH} at 64 K.

Conditions	T/ K	n/ 10^{16}cm^{-3}	[HC(O)OCH$_3$]/ 10^{13} cm^{-3}	$k_{OH}(T)$ [a]/ 10^{-11}cm^{3}s^{-1}	$k_{OH}(T)$/ k_{OH}(64K)
A	22.4 ±1.4	17.2±1.6	0.20-3.00	11.9±0.36	10.3
B	42.5±1.3	5.22±0.33	0.62-9.20	4.39±0.52	3.8
C	51.6±1.7	4.17±0.35	0.77-9.20	2.51±0.30	2.2
D	64.2±1.7	2.24±0.15	0.54-9.70	1.16±0.12	1

[a] Uncertainties are ±2σ, statistical and 10% due to systematic errors

Table 4. Literature values of the Arrhenius parameters, $k_{OH}(T) = A \exp(-E_a/RT)$, and experimental room temperature rate coefficient for the titled reaction.

$T/$ K	$k_{OH}(298K)/$ 10^{-13} cm^{3}s^{-1}	$A/$ 10^{-12} cm^{3}s^{-1}	$(E_a/ R)/$ K	Reference
296	2.27±0.34			Wallington *et al.* [23]
298	1.77±0.28			Good *et al.* [24]
298	1.83±0.33			Szilagyi *et al.* [25]
233 - 372	1.84	0.854±0.198	461±70	Le Calvé *et al.* [26]
880-1344	-	42.5	2026	Lam *et al.* [27]